

Design, Commissioning and Operation of the CTF3 Phase Feedforward System

J. Roberts,^{1, 2,*} P. Skowronski,² P. Burrows,¹ G. Christian,¹ R. Corsini,² A. Ghigo,³ F. Marcellini,³ and C. Perry¹

¹*John Adams Institute (JAI), University of Oxford,*

Denys Wilkinson Building, Keble Road, Oxford, OX1 3RH, United Kingdom

²*The European Organization for Nuclear Research (CERN), Geneva 23, CH-1211, Switzerland*

³*Laboratori Nazionali di Frascati (LNFN), Via Enrico Fermi, 40, 00044 Frascati RM, Italy*

(Dated: October 19, 2017)

Abstract

I. INTRODUCTION

A major challenge is the synchronisation of the arrival of the drive and main beams at the power-extraction and transfer structures to better than 50 fs rms. This requirement limits the luminosity loss, resulting from subsequent energy errors of the main beams, to less than 1% of the design value [?]. In the CLIC design the incoming drive-beam phase jitter cannot be guaranteed to be better than 2° [1]. A mechanism to improve the phase stability by an order of magnitude is therefore required. The correction must be applied to the full drive beam pulse length and have a bandwidth exceeding 17.5 MHz [2].

This is implemented via a ‘phase feed-forward’ (PFF) system which measures the incoming beam phase and provides a correction to the same beam pulse after it has traversed the turnaround loop (TA in Fig. ??). The incoming beam phase is measured in two upstream phase monitors (ϕ_1, ϕ_2). While the beam transits the turnaround loop a phase-correction signal is evaluated and used to drive fast, high power amplifiers; these drive two electromagnetic kickers (K_1, K_2) which are used to alter the beam transit time in a four-bend chicane. A downstream phase monitor (ϕ_3) is used to measure the effect of the correction.

The beam time of flight between ϕ_1 and K_1 is around 380 ns. The total cable delay for the PFF correction signals is shorter, around 250 ns. The correction in the chicane can therefore be applied to the entirety of the beam pulse measured at the PFF input (ϕ_1), provided that the hardware latency is less than 130 ns. Significant hardware challenges include the resolution and bandwidth of the phase monitors, and the power, latency and bandwidth of the kicker amplifiers. A low latency digitiser/feedforward controller is also required.

Key results from the CTF3 PFF system have previously been published in [REF]. This paper presents a more detailed description of the design and commissioning of the system - the hardware, the optics, the correction timing, and additional results.

CLIC intro/PFF system.

CTF3 layout, parameters etc.

CTF PFF system.

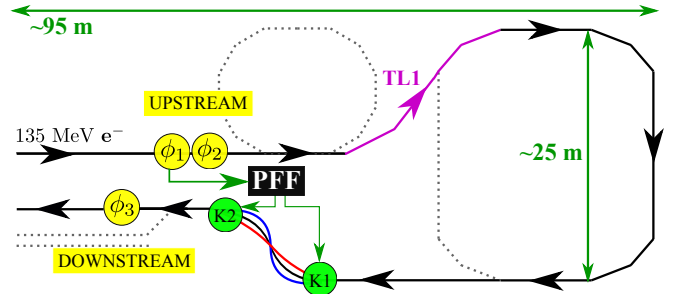


FIG. 1: Schematic of the PFF prototype at CTF3, showing the phase monitors (ϕ_1, ϕ_2 and ϕ_3) and kickers (K_1 and K_2). The black box PFF represents the calculation and output of the correction, including the phase monitor electronics, feedforward controller and kicker amplifiers. Dashed lines indicate beam lines that are not used during PFF operation. Bunches arriving early at the upstream monitor (ϕ_1) are directed on to longer trajectories in the correction chicane (blue), and bunches arriving late on to shorter trajectories (red).

II. HARDWARE

A. Phase Monitors

Three phase monitors were installed at CTF3 for the PFF prototype – two neighbouring monitors upstream, ϕ_{u1} and ϕ_{u2} , and one downstream of the correction chicane, ϕ_d . Fig. 2 shows the installation of the upstream phase monitors in the beam line. The upstream monitors are used to provide the PFF input (typically ϕ_{u1}), and to measure the phase monitor resolution. The notation ϕ_u will be used where the distinction between the measurements at ϕ_{u1} and ϕ_{u2} is unimportant. The downstream monitor, ϕ_d , is used to measure the effect of the PFF correction.

The phase monitors are cylindrical cavities with an external device length of approximately 19 cm and an internal diameter of 23 mm. Small ridges (notch filters) in the cavity create a volume resonating at 12 GHz (the CLIC drive beam frequency) which contains the beam induced fields and reflects any stray 12 GHz fields. The signals are extracted through horizontal and vertical pairs of rectangular waveguides, before transitioning to $50\ \Omega$ coaxial cable via RF feedthroughs [?]. The cavities support the

* Corresponding author Jack.Roberts@cern.ch

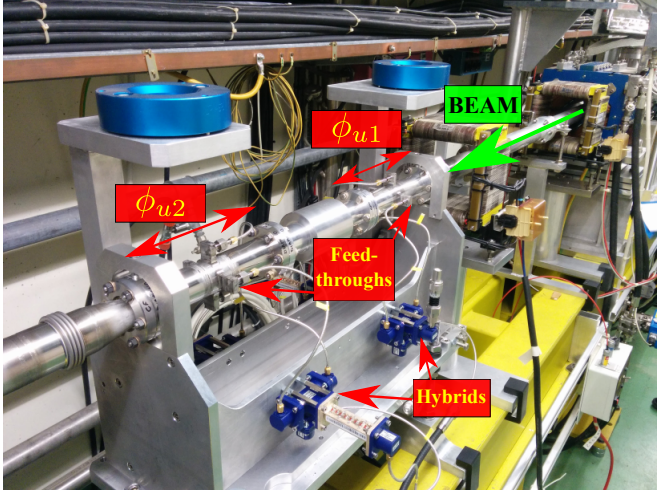


FIG. 2: The installation of the upstream phase monitors (ϕ_{u1} and ϕ_{u2}) in the beam line.

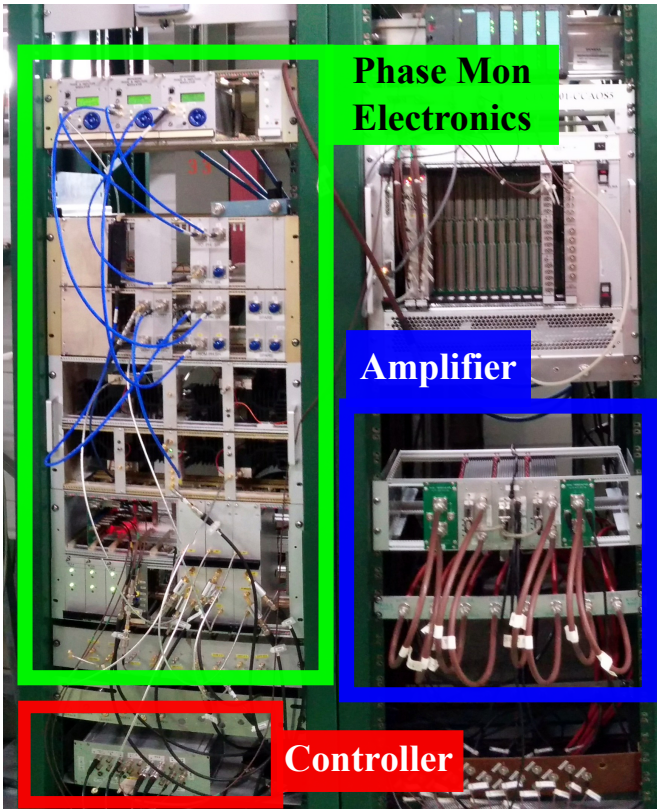


FIG. 3: The two racks containing the PFF system hardware – the phase monitor electronics, feedforward controller and the kicker amplifiers.

TM01 monopole and TE11 dipole modes. The position dependent dipole mode is removed by summing the pair of vertical outputs in 180 degree hybrids. The horizontal pair is instrumented in the same way but typically is not used.

The electronics used to extract the phase measurement

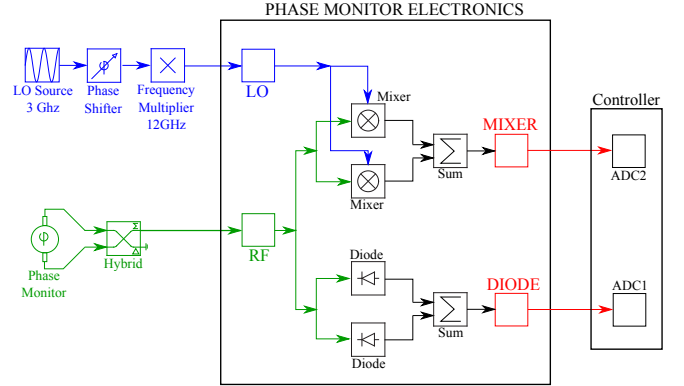


FIG. 4

from the cavity signals are installed on the floor above the machine hall in the CTF3 “klystron gallery”, alongside the other hardware used for the PFF system (Fig. 3). Each set of electronics produces two outputs - a phase dependent “mixer” signal, and a power dependent “diode” signal.

The beam induced signal from the cavities is down-mixed with a 12 GHz local oscillator (LO) to create the mixer output. The LO is generated from a common 3 GHz source that is phase-locked to the CTF3 drive beam. Each set of electronics has dedicated frequency multipliers, to increase the LO frequency to 12 GHz, and phase shifters, used for calibrations (see below). To be able to operate the mixers at low power (to improve linearity) whilst maintaining a large signal to noise ratio (to improve resolution) eight separate mixers and diodes are used in each set of electronics [?]. The inputs are split between the eight mixers and diodes, with the final two outputs being the sum of the individual mixer and diode signals. Fig. 4 shows a simplified example of this with two mixers and diodes.

The diode output was intended to be used to power normalise the mixer output. However, an unforeseen design issue with the electronics resulted in the diodes saturating at a much lower input voltage than the mixers (Fig. 5). To be able to achieve the best possible resolution from the mixers, the electronics were operated with the diodes saturated, and the diode outputs were not used in the phase reconstruction as envisaged. As a consequence, calibrations had to be repeated regularly to account for any differences in output power from the cavities resulting from changes to the beam setup.

The phase, $\phi(t)$, was therefore calculated from the “Mixer” outputs as follows:

$$\text{Mixer}(t) = A \sin[\phi(t)] + d \quad (1)$$

$$\phi(t) = \arcsin\left(\frac{\text{Mixer}(t) - d}{A}\right) \quad (2)$$

Two calibration constants are needed – A and d . A is the fitted (power dependent) amplitude of the sinusoidal mixer output, and d is the asymmetry or offset between the maximum and minimum mixer output.

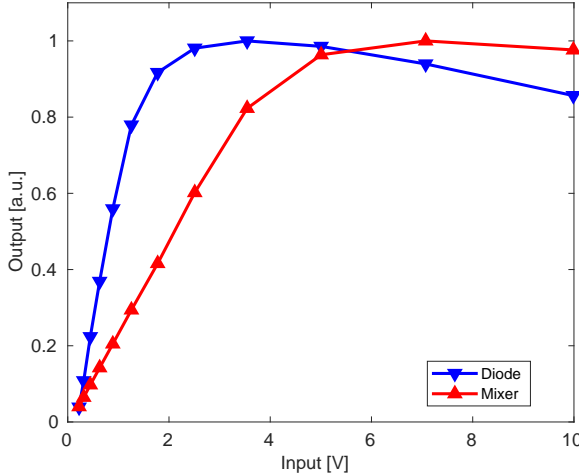


FIG. 5: Electronics diode and mixer output amplitudes (normalised with respect to their peak output) versus the input voltage.

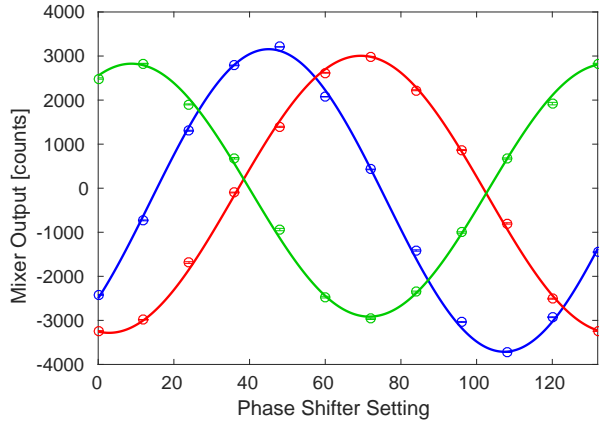


FIG. 6

Point by point and mean resolution

Bandwidth

Position dependence

Figure ?? shows the results of a horizontal position scan in the upstream phase monitors, with the phase plotted against the horizontal position in the BPM.

Taking the calculated position dependence of Mon 1 and Mon 2 this corresponds to only an additional measured phase jitter of roughly 0.04° , using the larger dependence in the horizontal plane. This is small compared to the phase monitor resolution

B. Feedforward Controller

The basic logic of the firmware is as follows. The ADC sampling and timing are defined by the input trigger and external 357 MHz clock. The ADC outputs are pro-

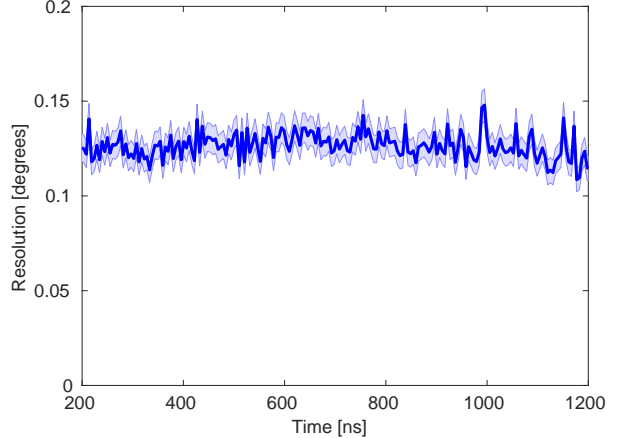


FIG. 7

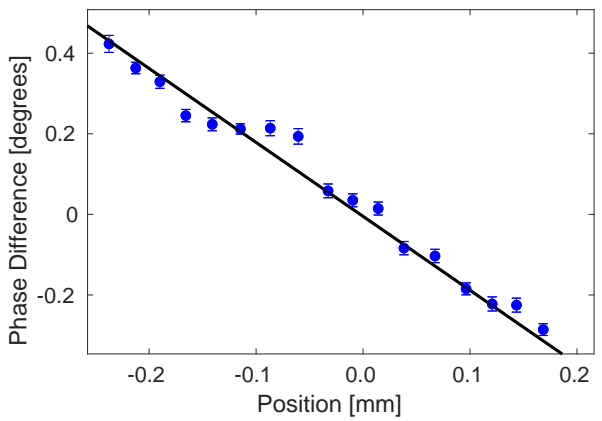


FIG. 8

cessed continuously on the FPGA, including the addition of channel offsets and the application of filters. Then the processed ADC 2 (Mixer) output is split in two, creating the two parallel strands that become the DAC 1 and DAC 2 outputs. Note that, instead of using arcsine, the Mixer value is used directly in the calculation, thereby assuming the small angle approximation. Prior to being sent to the DACs the two output strands are multiplied by their corresponding gain factors, as set in the DAQ. An additional delay can be added to the DAC outputs, allowing the synchronisation of the correction with the beam to be adjusted. The two calculated DAC outputs are connected to the amplifier drive inputs, where they are amplified and eventually output to the kickers to deflect the beam and correct the phase. The overall latency of the FONT5a board, from the arrival of the signal at the ADCs to the output of the calculated correction at the DACs, is around 22 clock cycles (at 357 MHz) or 60 ns [?].

In the PFF system the voltage sent to the kickers in the TL2 chicane (see Figures ?? and ??) is varied de-

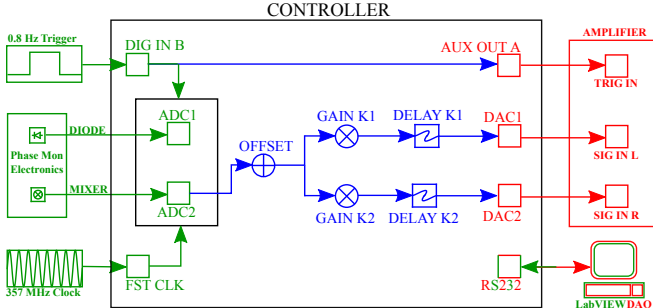


FIG. 9

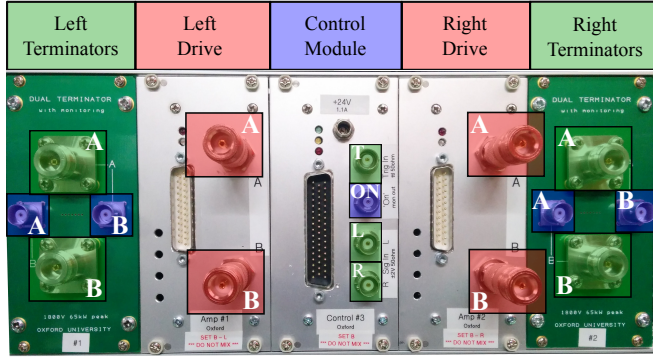


FIG. 10

pending on the upstream phase. The corrected downstream phase, ϕ_{PFF} , can therefore be simply modelled as subtracting the upstream phase, ϕ_u , from the initial downstream phase ϕ_d :

$$\phi_{PFF} = \phi_d - g\phi_u \quad (3)$$

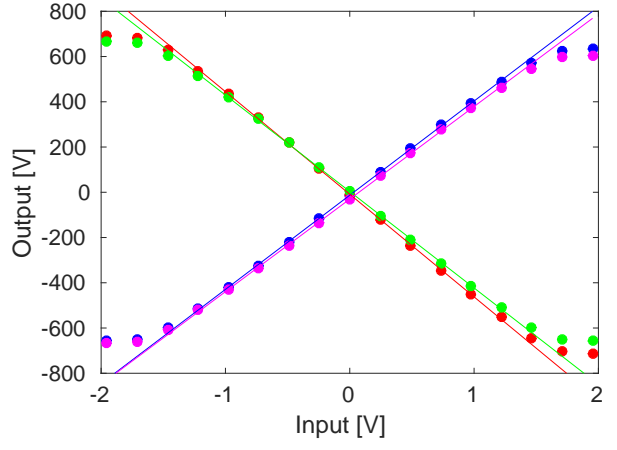
$$g = \rho_{ud} \left(\frac{\sigma_d}{\sigma_u} \right) \quad (4)$$

$$\sigma_{PFF} = \sigma_d \sqrt{1 - \rho_{ud}^2} \quad (5)$$

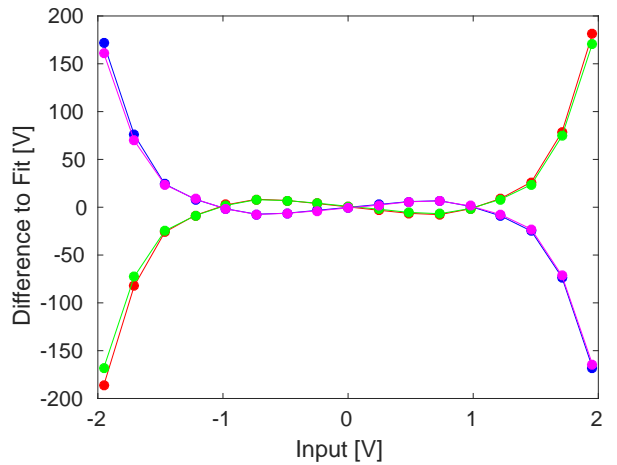
C. Amplifiers

The amplifier takes the two DAC signals from the FONT5a board and uses them to produce four high voltage outputs. These are connected to the downstream ends of the kicker strips (two kickers and two strips per kicker gives four connections at the downstream ends in total), creating the potential difference between the strips that deflects the beam in order to correct the phase. The returning signals from the upstream ends of the kicker strips are then terminated back at the amplifier.

The amplifier is purpose built for the PFF prototype, also at Oxford University, with further details of its design available in [?]. An annotated picture of its front panel is shown in Figure ?? and a simplified diagram



(a)



(b)

FIG. 11: test 11a

showing the flow of signals between the FONT5a board, amplifier and kickers is shown in Figure ???. The amplifier is installed in a standard 3U rack and has a modular design. It consists of five individual modules split between two sides, labelled left and right. The left side of the amplifier, which uses the DAC 1 output, powers the first kicker in the chicane, and the right side of the amplifier, which uses the DAC 2 output, powers the second kicker. Each side of the amplifier contains its own “drive module” and “terminator module”. Finally there is a central “control module” that is common to both sides of the amplifier.

Figure 11a shows the amplifier output, measured using the monitoring signals, at different constant input voltages sent from the FONT5a board between the minimum of -2V (-4095 DAC counts) and maximum of 2V (+4095 DAC counts). The amplitude of the monitoring signals is converted in to the amplifier output voltage using the approximate conversion factor of 115 [?]. All four amplifier outputs are shown (one for each strip of the two

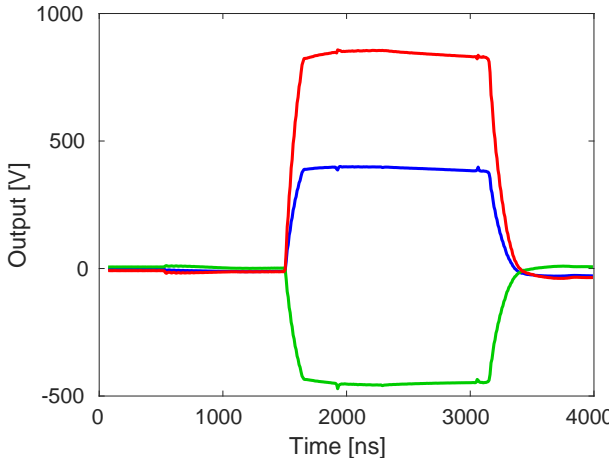


FIG. 12

kickers). The values plotted are the mean of the 480 ns central region of the whole 1400 ns output pulse.

The response of the amplifier is linear up to ± 1.2 V input voltage. Outside this range the amplifier clearly begins to enter saturation, in particular above input voltages of ± 1.7 V. The linear fits shown include only the points up to ± 1.2 V, in order to not be biased by the effects of saturation. Figure 11b shows the difference between the linear fit and the measured amplifier output across the full range of input voltages. A slight deviation from linearity in the ± 1.2 V range is also visible, although the maximum difference is only 10 V or a 3% relative error.

Figures ?? and ?? show the full $1.4 \mu\text{s}$ amplifier output with a constant input of $+1$ V (-1 V) applied to the left (right) amplifier respectively. Spikes in the signal just prior to 2000 ns and after 3000 ns on the time axis as seen in the plots are pickup on the kicker strips induced by the beam. For a constant input voltage the output voltage along the pulse varies by up to 88 V peak-to-peak (mean 12 V) for the left amplifier or 93 V peak-to-peak (mean 14 V) for the right amplifier. As a relative difference, this corresponds to approximately a 6 % peak-to-peak, or 1 % mean, variation along the pulse.

Brief design

Linearity

Pulse shape

D. Kickers

The two electromagnetic kickers provide the phase correction in the PFF system by deflecting the beam on to longer or shorter paths in the TL2 chicane (see Figure ??). They have been designed and built by INFN, Italy [?], based on a similar design used at the DAΦNE collider [?]. A schematic of the kicker design is shown in Figure 13. It consists of two parallel conducting strips

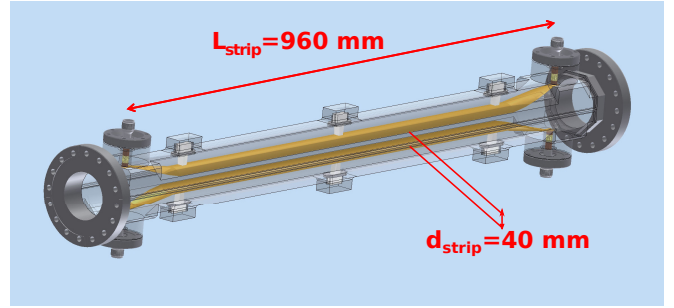


FIG. 13

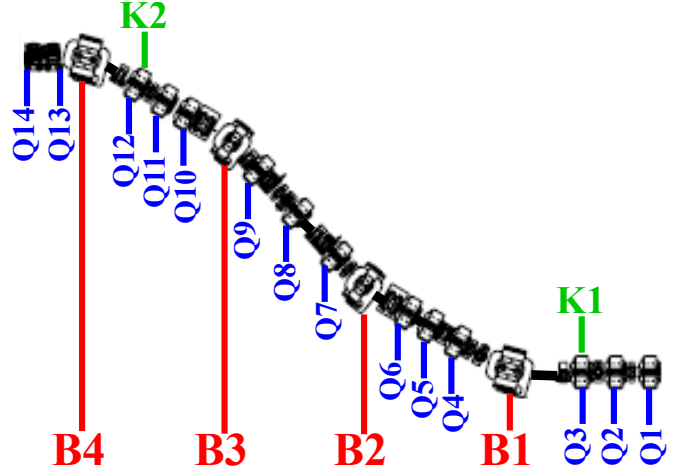


FIG. 14

placed along the left and right side of the beam pipe. Each strip is approximately one metre in length and the horizontal separation between the strips is 40 mm. The strips are tapered at their ends to reduce coupling impedance (to reduce the voltage induced on the strips by the beam) [3].

Brief design, cable connections etc.

III. OPTICS

A. Correction Chicane

The PFF system places new constraints on the optics of the correction chicane, the lattice of which is shown in Fig. 14. The chicane has a dog-leg shape containing 4 dipoles, with the external pair (B1 and B4) bending the beam through $\pm 31^\circ$ and the internal pair (B2 and B3) through $\pm 17^\circ$. Each section of the chicane between the dipoles includes a triplet of quadrupoles. The total length of the chicane, including the quadrupole triplet upstream of B1, is around 15 m.

The pre-existing TL2 chicane was already densely packed with magnets, and to maintain the functionality of the lattice for routine operation at CTF3 elements could not be removed. Space for the two PFF kickers (K1

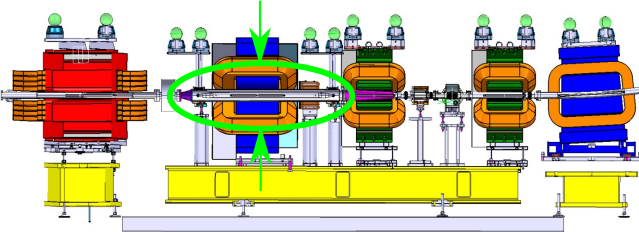


FIG. 15

and K_2) was made available by rearranging quadrupoles in the line, moving quadrupoles with a wide aperture (Q_3 and Q_{12}) prior to the first (B_1) and last (B_4) dipole in the chicane. The kickers are installed inside the aperture of these quadrupoles (Fig. 15).

New optics for the TL2 line, maintaining the previous matching constraints required for normal operation and adding the new PFF constraints, were created using the CTF3 MADX model. The accuracy of the model for the rearranged line was verified and improved in a series of kick-response measurements [REF]. Relying on the pre-existing chicane layout forced several compromises in the chicane optics.

The original optics constraints include - matching combiner ring extraction and CLEX injection, dispersion closure and minimised, beta functions small/smooth. The additional PFF constraints ensure the phase (path length) dependence on the kicker voltages, and that the beam orbit downstream of the chicane is closed.

The rms beam energy spread at CTF3 is at the 1% level. The beam pipe in the correction chicane has a diameter of 10 cm to give a large acceptance for the dispersion component of the beam size. However, the aperture of the PFF kickers is only 2 cm. The dispersion must be closed at the chicane exit and minimised at K_2 (K_1 is prior to the chicane in a dispersion free region).

The correction range of the PFF system, or the dependence of the beam phase on the angular deflection applied at K_1 , is defined by the transfer matrix coefficient R_{52} between the two kickers:

$$\phi_{K2} = \phi_i + R_{52}x'_{K1} \quad (6)$$

Maximising R_{52} has the unfortunate consequence of increasing the dispersion, thus the optics must be a compromise that achieves a reasonable correction range whilst keeping the dispersion small enough to avoid beam losses.

The dispersion and phase shift for a 1 mrad kick at K_1 in the matched optics for the chicane are shown in Fig.[REF] and Fig.[REF] respectively. An R_{52} value of 0.74 m is achieved (corresponding to a phase shift of -10.6° per mrad at K_1) with a dispersion of [val] at K_2 . With this dispersion approximately [val] sigma of the beam energy distribution fits within the K_2 aperture.

The last two figures, ?? and ??, show the effect of kicking the beam with the PFF kickers. A deflection of

+1 mrad is applied from the first kicker, and -1 mrad from the second kicker. This leads to a peak horizontal orbit offset of 3.5 mm inside the horizontal chicane. The orbit is closed at the 10^{-7} level following the chicane, so that the beam's trajectory following the PFF system is independent of the applied kick.

Finally, the R_{52} value between the two kickers is 0.74 m. This defines the phase shift resulting from kicking the beam in the chicane, which is the key figure of merit for the PFF system. As shown in Figure ?? a kick of 1 mrad provides a phase shift of -10.6° in this optics. This is converted in to the actual range of the PFF system taking in to account the specifications of the kicker amplifiers in Chapter ???. Verifications of the performance of the optics are presented in Chapters ?? and ??.

B. Phase Propagation

As in Eq.[ref] the corrected downstream phase jitter that the PFF system can achieve depends on the correlation between the upstream (input) phase and the initial downstream phase. This correlation is determined by the phase monitor resolution and any additional beam phase jitter introduced in-between ϕ_u and ϕ_d . In the first measurements with the new correction chicane optics (such as Fig.17) the correlation was below 40% and the downstream phase jitter more than two times larger than upstream.

One constraint that could not be met in conjunction with the other chicane optics requirements was for the transfer matrix element R_{56} to be zero. R_{56} describes the dependence of the phase on the beam energy, to first order, as follows:

$$\phi_d = \phi_u + R_{56} \frac{\Delta p}{p} \quad (7)$$

Where R_{56} is the R_{56} coefficient between the upstream and downstream monitors, and $\Delta p/p$ is the fractional energy offset.

As seen in Figure ?? the R_{56} transfer matrix coefficient across the horizontal chicane is -0.18 m. As other beam lines at CTF3 nominally have $R_{56} = 0$, the total R_{56} between ϕ_u and ϕ_d is also -0.18 m. This leads to additional energy dependent phase jitter in ϕ_d that is not present in ϕ_u .

The effect of this is shown in Fig. 18, in which the phase is plotted versus the beam energy (calculated using the beam position in a dispersive BPM). A correlation of [val] between the upstream phase and the beam energy is amplified to [val] downstream.

From Equations [val] and [val] the effect of R_{56} on the correlation and the PFF performance can be derived [REF]. Excluding the phase monitor resolution, the corrected downstream phase jitter that can be achieved is given by:

$$\sigma_{PFF} = |R_{56}| \sigma_p \sqrt{1 - \rho_{up}^2} \quad (8)$$

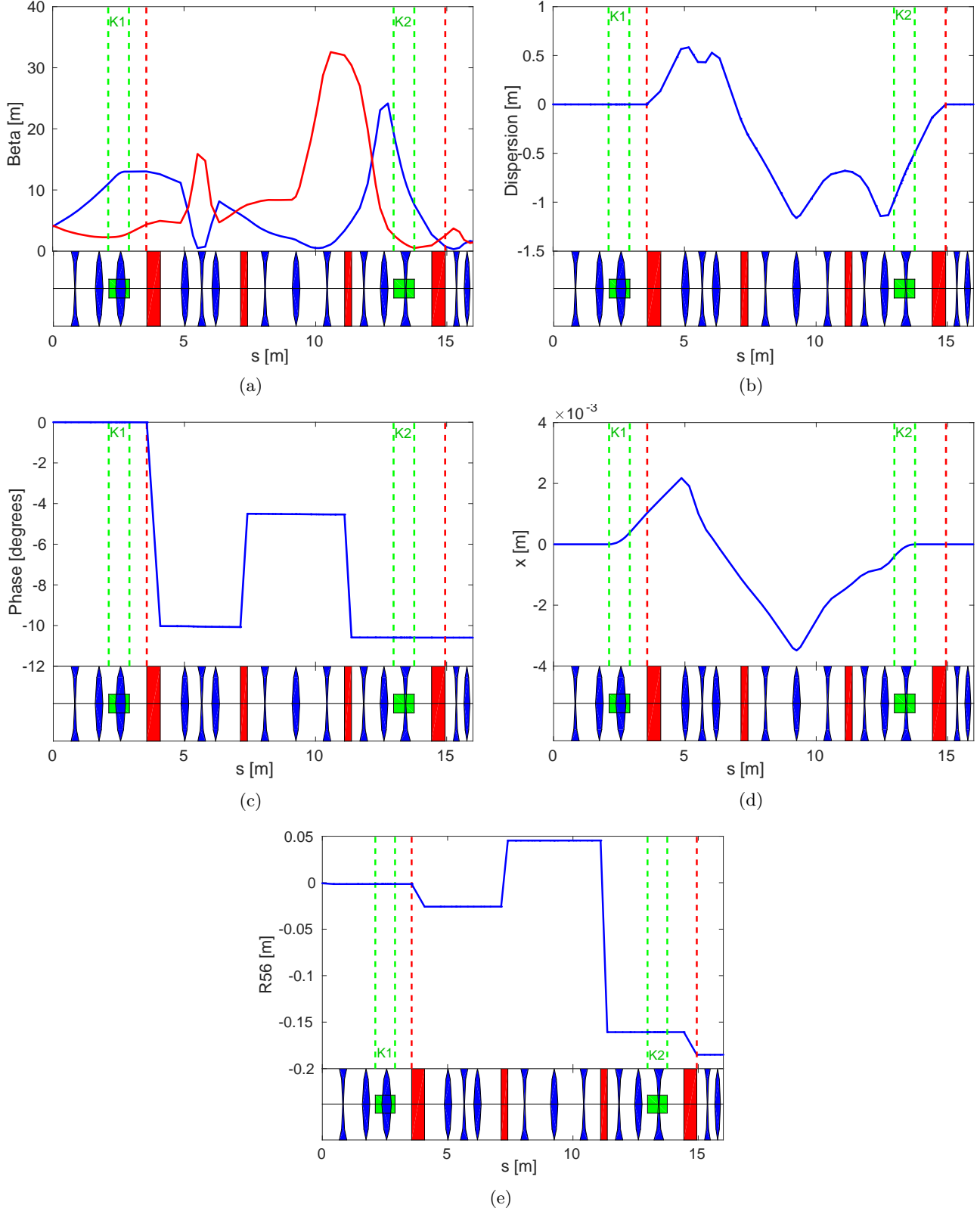


FIG. 16: Optics for the correction chicane.

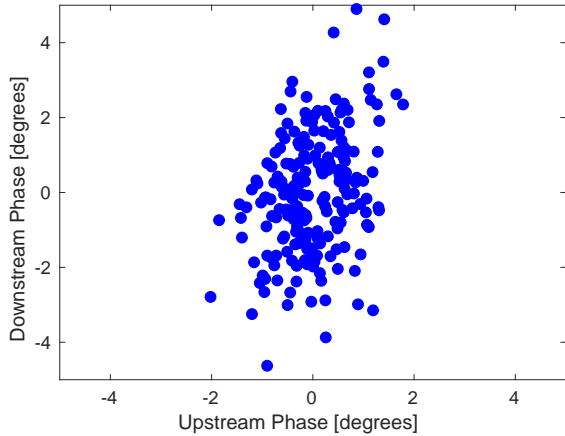


FIG. 17

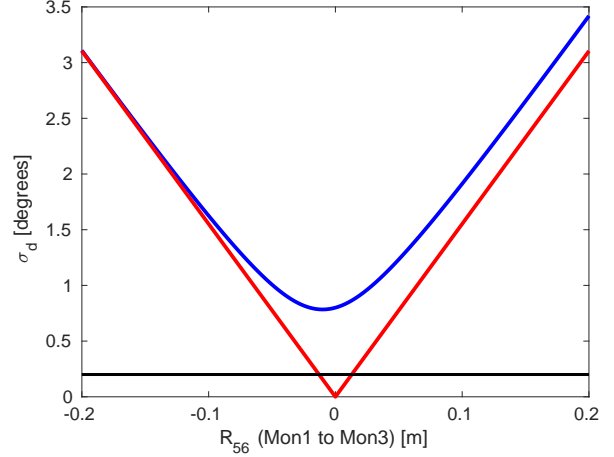


FIG. 19

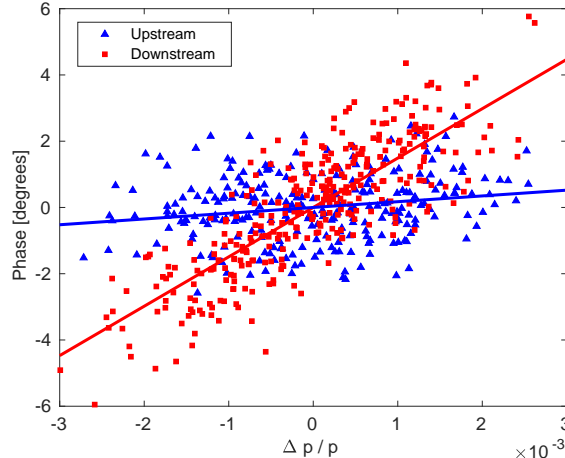


FIG. 18

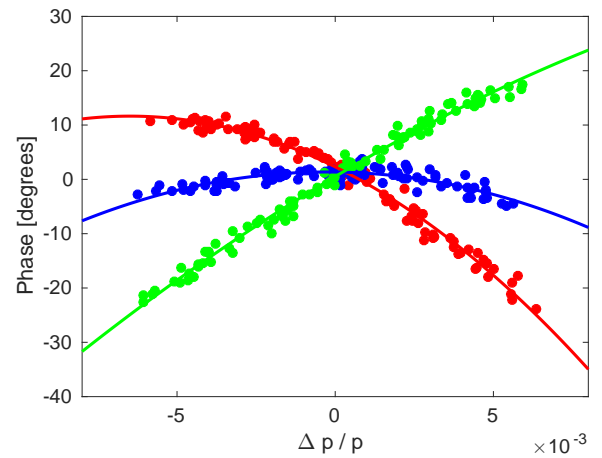


FIG. 20

Where σ_p is the beam energy jitter (typically [val] at CTF3) and ρ_{up} is the correlation between the upstream phase and the beam energy (typically [val]). Fig.19 shows the dependence of the initial and corrected downstream phase jitter on the R_{56} value. The slight asymmetry between positive and negative R_{56} values is caused by the non-zero correlation between the upstream phase and the beam energy. To reduce a typical initial beam jitter of 0.8° at CTF3 to the CLIC target of 0.2° , the R_{56} value between the upstream and downstream monitors must be less than [val].

To compensate, messed around with TL1... R56 scan...

Optimal R_{56} value not constant... correlation variations along pulse... hinted at higher order effects... Second order phase-energy dependence in the optics is described using the T_{566} matrix coefficient:

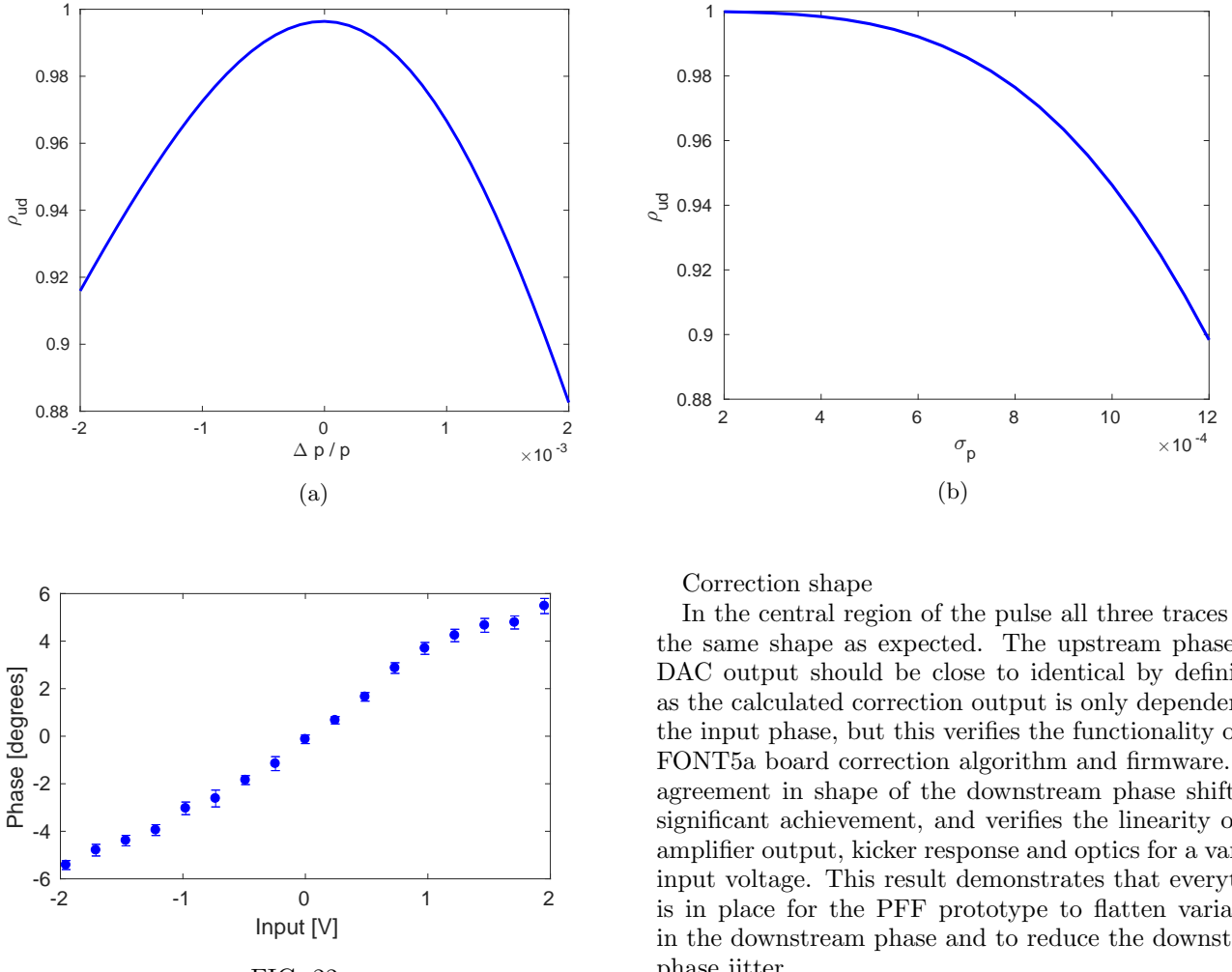
$$\phi_d = \phi_u + R_{56} \left(\frac{\Delta p}{p} \right) + T_{566} \left(\frac{\Delta p}{p} \right)^2 \quad (9)$$

Fig. 20 shows the dependence of the mean downstream

phase on the beam energy for three different R_{56} values set in TL1: -0.1 m, 0.075 m and 0.3 m. The beam energy was varied during the data taking period, and the second order term becomes clear.

Figs. 21a and 21b shows the effect of T_{566} on the correlation for different beam energy offsets and beam energy jitters respectively. In each case it is assumed the first order R_{56} has been completely cancelled using TL1. energy jitter/offset [val] assumed.

In optimal conditions CTF3 energy jitter as low as [val] and variations along pulse below [val], which means not a limiting factor to achieve 0.2 degrees. But the sensitivity to energy drifts made it difficult/impossible to maintain peak PFF performance on long time scales. CLIC application would require R_{56} and T_{566} to be zero in the turnarounds.



IV. SYSTEM SETUP AND VERIFICATION

A. Correction Range

Figure ?? shows the measured mean phase shift in the downstream phase monitor across the full ± 2 V input range of the amplifier. Constant DAC outputs in 17 steps between -4095 counts (-2 V) and +4095 counts (+2 V) were used to drive the amplifier. For each amplifier input voltage 100 beam pulses were acquired in interleaved mode in order to reduce the sensitivity to any drifts in beam phase between data points. The phase plotted in Figure ?? is the difference between the 50 beam pulses with the DAC output enabled (non-zero amplifier input) and the 50 beam pulses with the DAC output disabled (0 V amplifier input). At the maximum amplifier input voltage of 2 V the phase is shifted by $5.5 \pm 0.3^\circ$. The fitted phase shift per Volt input is $3.5 \pm 0.1^\circ$ in the ± 1.2 V linear range of the amplifier.

The measured correction range is shown in Fig.22. Correction range agrees with expected range

Correction shape

In the central region of the pulse all three traces have the same shape as expected. The upstream phase and DAC output should be close to identical by definition, as the calculated correction output is only dependent on the input phase, but this verifies the functionality of the FONT5a board correction algorithm and firmware. The agreement in shape of the downstream phase shift is a significant achievement, and verifies the linearity of the amplifier output, kicker response and optics for a varying input voltage. This result demonstrates that everything is in place for the PFF prototype to flatten variations in the downstream phase and to reduce the downstream phase jitter.

The agreement in shape holds for times between around 900 ns and 1375 ns as indicated on the figure, and this defines a 475 ns portion of the pulse within which the applied correction should be close to optimal. Outside this range the large phase sag along the pulse leads to the correction being saturated – the maximum possible DAC output (2 V) is applied and the shape can no longer be corrected. It can also be seen that the measured downstream phase shift saturates earlier than the applied DAC output. This is because the amplifier begins to saturate at input voltages below 2 V, as seen in Figure 11a.

B. Correction Shape

The PFF system removes intra-pulse phase variations as well as inter-pulse variations.

The input upstream phase, calculated DAC output and the observed difference in the downstream phase resulting from the applied kick are all shown. The downstream phase trace shows the difference between subsequent pulses with the correction on and off (using the interleaved correction mode). Each trace is scaled, aligned

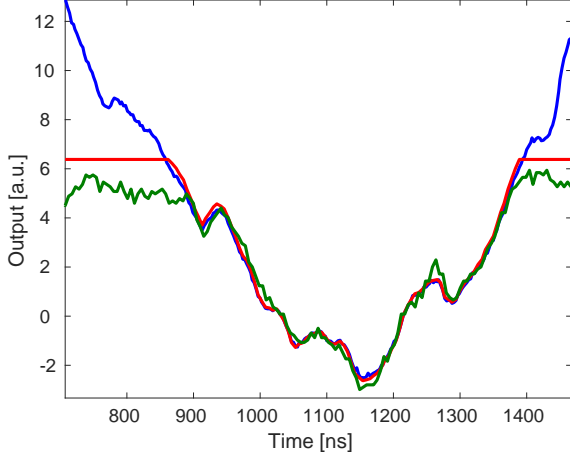


FIG. 23

in time and sign flipped where appropriate to make a comparison between the shapes easier.

In the central region of the pulse all three traces have the same shape as expected. This verifies the linearity of the amplifier output, kicker response and optics for a varying input voltage. This result demonstrates that everything is in place for the PFF prototype to flatten variations in the downstream phase and to reduce the downstream phase jitter.

The agreement in shape holds for times between around 900 ns and 1375 ns as indicated on the figure, and this defines a 475 ns portion of the pulse within which the applied correction should be close to optimal. Outside this range the large phase sag along the pulse leads to the correction being saturated – the maximum possible DAC output (2 V) is applied and the shape can no longer be corrected. It can also be seen that the measured downstream phase shift saturates earlier than the applied DAC output. This is because the amplifier begins to saturate at input voltages below 2 V, as seen in Figure 11a.

C. Orbit Closure

Fig. 24 shows the orbit closure measured in the BPMs in and around the correction chicane. The BPM orbit is compared to the expected trajectory in the nominal optics for the chicane. The measurement and the model are in good agreement. A maximum horizontal offset of 1.5 mm inside the chicane is reduced to less than 0.1 mm after the chicane.

D. Correction Timing

To be able to correct intra-pulse phase variations the arrival of the amplifier drive voltage at the kicker strips

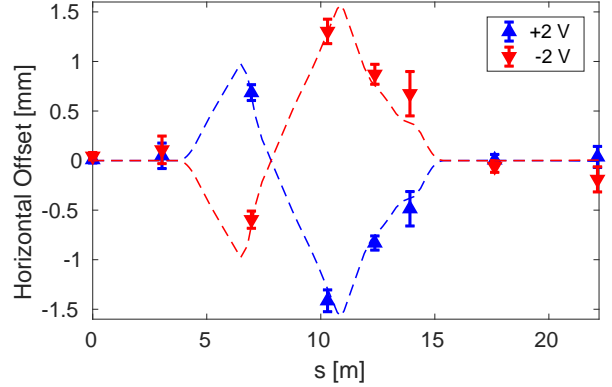


FIG. 24

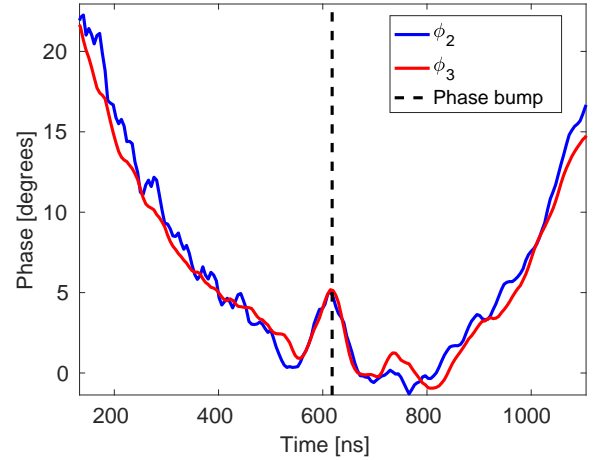


FIG. 25

must be precisely synchronised with the arrival time of the beam. The correction timing is controlled by the feedforward controller and has been optimised with beam based measurements, as presented here.

The waveforms of the klystrons were changed to produce a clear phase bump in the centre of the beam pulse. The bump is clearly visible in both ϕ_1 and ϕ_3 , as shown in Fig. 25. This feature was used to determine the necessary delay in the controller output in order to align the PFF correction (the kicker voltage) with the beam.

The PFF correction was applied in interleaved mode. The phase shift at ϕ_3 caused by the PFF system can then be calculated by taking the difference between the ‘PFF On’ and ‘PFF Off’ pulses in the dataset. For the optimal system setup this difference should be identical to the initial (‘PFF Off’) phase but with opposite sign.

Fig. 26 shows the difference (labelled ‘kick’) compared to the initial phase for four different controller output delays, zoomed in to the region of the pulse with the added phase bump. The differences are sign flipped and scaled to facilitate comparisons with the initial phase. Dashed lines indicate the time of the phase bump peak

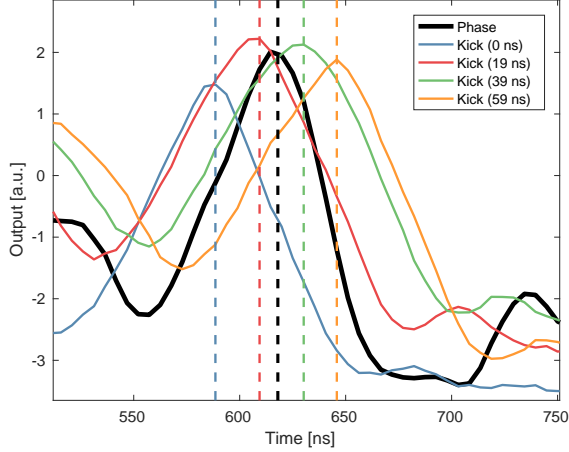


FIG. 26

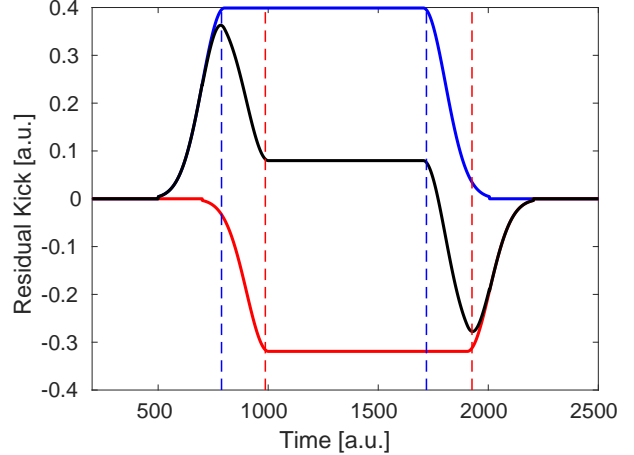


FIG. 28

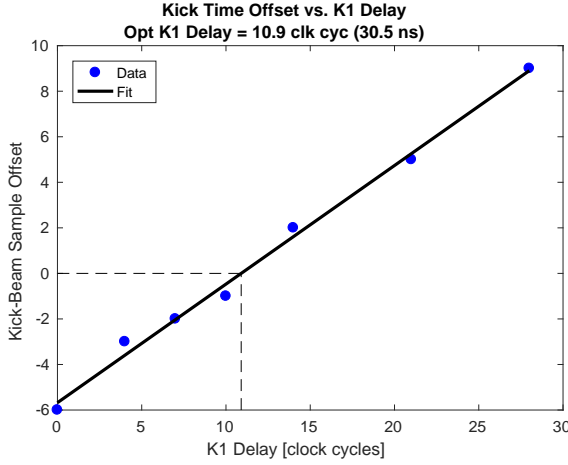


FIG. 27

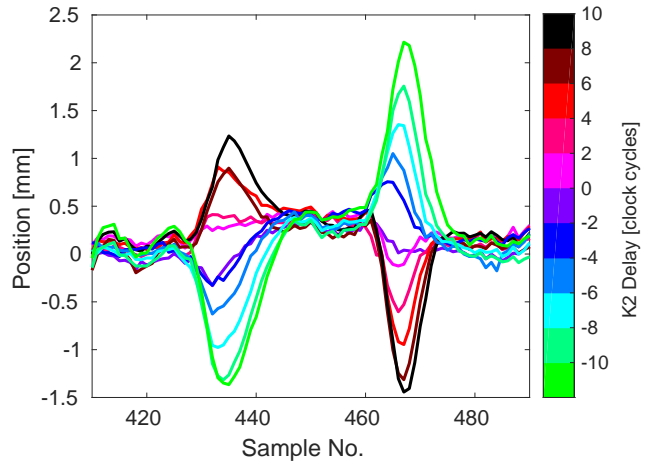


FIG. 29

in each case.

With the correction applied as soon as possible ('Kick 0 ns', blue) the phase bump in the applied kick arrives early, at 588 ns in the figure compared to 618 ns for the initial phase. This proves the PFF system meets the latency requirements, with a total system latency of around 350 ns compared to the 380 ns beam time of flight. As the output delay from the controller is increased, the phase bump in the applied kick overlaps and then trails its location in the initial phase. Fitting the difference in the peak positions vs. the output delay yields an optimal controller delay of 31 ± 4 ns (Fig. 27).

The previous measurement verifies the timing of the correction signal applied to the first kicker (K_1), which provides the phase shift in the chicane. The second kicker (K_2) ensures the beam orbit downstream of the chicane is unaffected by the PFF correction, but has a negligible effect on the beam phase. The beam time of flight between the kickers is about 36 ns, thus the PFF correction voltage must arrive at K_2 36 ns later than the correction

at K_1 . If this is not the case the PFF system will cause horizontal position offsets downstream of the chicane.

Fig. 28 illustrates the effect of the correction not being synchronised with the beam at both kickers. A constant voltage is applied to the kickers, as shown in red and blue. The total kick, the sum of the two, is in black and should be zero for the whole pulse duration in the ideal PFF setup. A time offset between the kicker voltages with respect to the beam leads to a large residual kick at the start and end of the pulse. If the kicker voltages have different magnitudes there is also a constant offset in the central portion of the pulse.

The amplifier-to-kicker cables for K_2 are longer than the K_1 cables to compensate for additional beam time of flight. The correction output delay for each kicker can also be fine-tuned independently on the feedforward controller.

To verify the timing of the K_2 correction output the feedforward controller was used to apply a constant kick to a 168 ns portion of the pulse. The kick was applied in

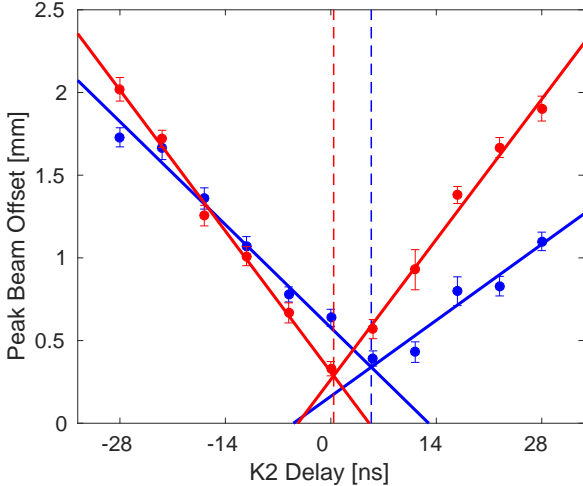


FIG. 30

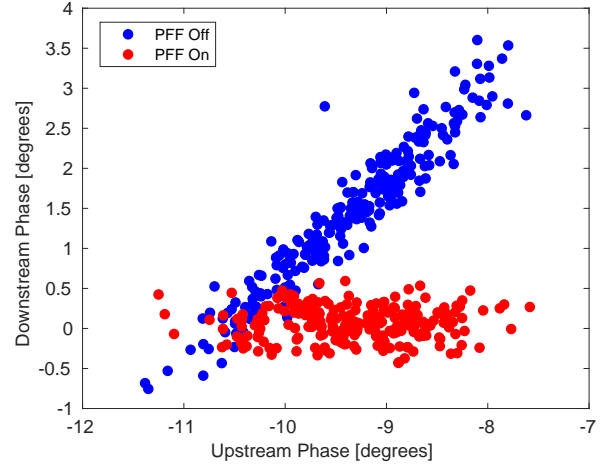


FIG. 32

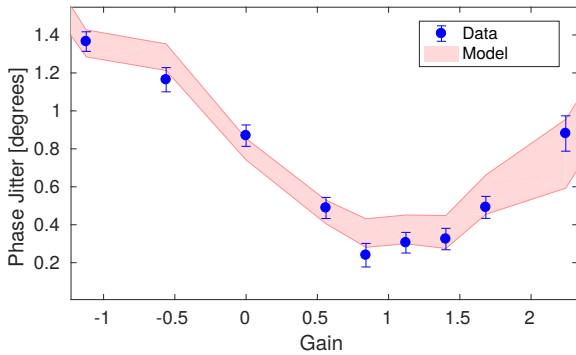


FIG. 31

interleaved mode, with the horizontal position difference between the PFF Off and PFF On pulses measured in a BPM downstream of the chicane. Fig. 29 shows this difference for different delays applied to the K_2 correction output with respect to the K_1 output, ranging from -28 ns to $+28$ ns. The response is similar to the simulated example in Fig. 28, as expected.

The optimal delay for the K_2 correction output minimises the size of the peaks resulting from residual kicks, and this is fitted for the peaks at both the leading and trailing end of the pulse in Fig. 30. The fitted value is 1.4 ± 1.7 ns. During operation of the PFF system the K_2 output was typically delayed by 2.8 ns with respect to K_1 . This is the minimum non-zero delay that can be applied by the feedforward controller (equivalent to one time period of the 357 MHz ADC clock frequency).

E. Correction Gain

The PFF system acts to remove the ϕ_1 phase, multiplied by a ‘gain’ factor, from the phase at ϕ_3 . If the

phases at ϕ_3 and ϕ_1 are fully correlated, and the jitters are identical, the optimal system gain is unity. In practice the gain is chosen to achieve optimal performance for real beam conditions. A representative gain scan is shown in Fig. ???. The optimal gain is typically in the range 0.9 – 1.3 . Also shown in Fig. ?? is a prediction of the corrected phase jitter at ϕ_3 , using a simple model including the initial beam phase jitters at ϕ_1 and ϕ_3 , the upstream-downstream phase correlation, and the gain [4]. The model reproduces the data.

V. RESULTS

A. Correction of Mean Phase Jitter

The effect of the PFF system on the pulse-to-pulse jitter, i.e. the jitter on the mean phase of each beam pulse, is shown in Fig. ?? for a dataset of around ten minutes duration. The pulse-to-pulse phase jitter is reduced from $0.92 \pm 0.04^\circ$ to $0.20 \pm 0.01^\circ$, meeting CLIC-level phase stability. The system acts to remove all correlation between the upstream and downstream phase, reducing an initial correlation of $96 \pm 2\%$ to $0 \pm 7\%$ for this dataset. Given the incoming upstream phase jitter and measured upstream-downstream correlation, the performance is consistent with the theoretically predicted correction of $0.26 \pm 0.06^\circ$.

Best mean jitter

B. Correction of Pulse Shape

The PFF system simultaneously corrects pulse-to-pulse phase jitter and phase variations within the $1.2 \mu\text{s}$ beam pulse at CTF3. Fig. ?? shows the effect of the PFF system on the intra-pulse phase variations. The PFF system was operated in interleaved mode, with the

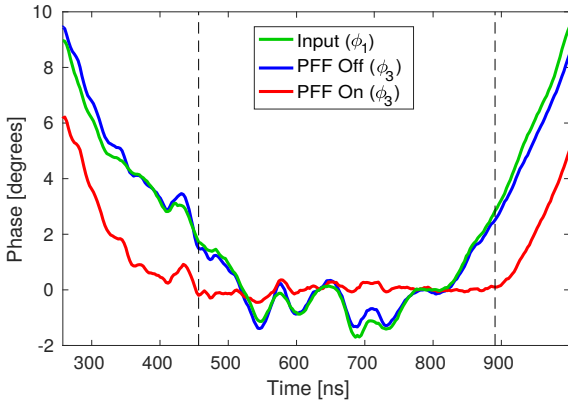


FIG. 33

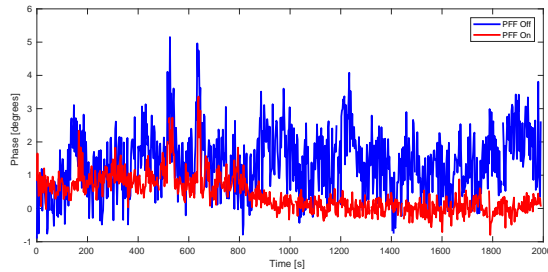


FIG. 34

correction applied to alternating pulses only. This allows the initial ('PFF Off') and corrected ('PFF On') downstream phase at ϕ_3 to be measured at the same time. The ϕ_1 (PFF input) phase is also shown for comparison.

Approximately 440 ns portion of the pulse is within the $\pm 6^\circ$ dynamic range of the PFF system, and can be corrected to zero nominal phase. This time duration for the full correction exceeds the CLIC drive-beam pulse length of 240ns and in any case the CLIC design avoids such a large phase sag [1]. Vertical dashed lines in Fig. ?? mark the 440 ns portion of the pulse where full correction is possible.

Within the range the PFF system flattens the phase, and almost all variations are removed. Residual offsets are still present where there are small uncorrelated differences between the initial phase at ϕ_1 and ϕ_3 . The average

intra-pulse phase variation (rms) over the dataset is reduced from $0.960 \pm 0.003^\circ$ (PFF off), to $0.285 \pm 0.004^\circ$ (PFF on).

Best shape

C. Long Term Results

Long term correction and issues.

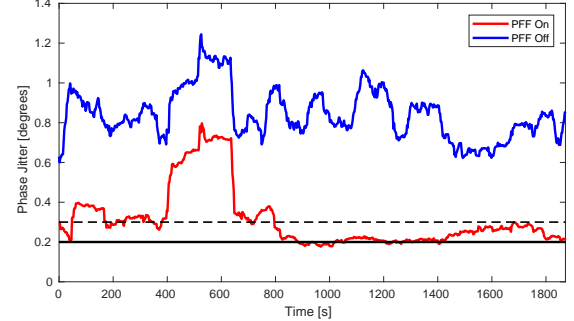


FIG. 35

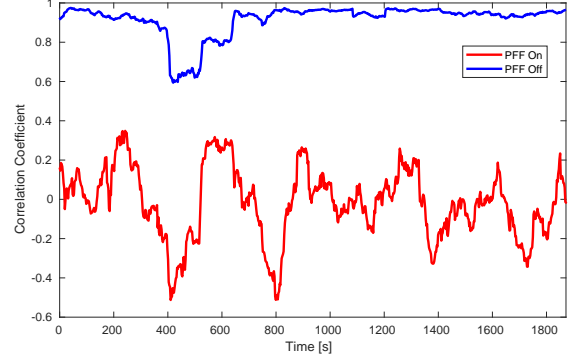


FIG. 36

VI. CONCLUSIONS

ACKNOWLEDGMENTS

-
- [1] M. Aicheler *et al.*, "A multi-TeV linear collider based on CLIC technology: CLIC conceptual design report," CERN-2012-007 (2012).
 - [2] A. Gerbershagen *et al.*, Phys. Rev. AB **18**, 041003 (2015).
 - [3] A. Ghigo *et al.*, in *Proceedings of IPAC2011*, Vol. TUPC007 (San Sebastian, Spain, 2011) pp. 1000–1002.
 - [4] J. Roberts, *Development of a Beam-based Phase Feedforward Demonstration at the CLIC Test Facility (CTF3)*, DPhil thesis, University of Oxford (2016).